STRUCTURAL CONTROL AND HEALTH MONITORING
Struct. Control Health Monit. 2008; **15**:1122–1142
Published online 19 March 2008 in Wiley InterScience
(www.interscience.wiley.com) DOI: 10.1002/stc.255

Incipient damage identification through characteristics of the analytical signal response

Giulio Cottone[1], Antonina Pirrotta[1,*,†] and Salvatore Salamone[1,2]

[1] *Dipartimento di Ingegneria Strutturale e Geotecnica, Università degli Studi di Palermo, Viale delle Scienze, 90128-Palermo, Italy*
[2] *NDE & Structural Health Monitoring Laboratory, Department of Structural Engineering, University of California, San Diego, 9500 Gilman Drive, M.C. 0085, La Jolla, CA 92093-0085, U.S.A.*

SUMMARY

The analytical signal is a complex representation of a time domain signal: the real part is the time domain signal itself, while the imaginary part is its Hilbert transform. It has been observed that damage, even at a very low level, yields clearly detectable variations of analytical signal quantities such as phase and instantaneous frequency. This observation can represent a step toward a quick and effective tool to recognize the presence of incipient damage where other frequency-based techniques fail. In this paper a damage identification procedure based on an adimensional functional of the square of the difference between the characteristics of the analytical theoretical and measured signal is proposed. Numerical examples, on a single degree of freedom system and of 3 degrees of freedom building model, prove the efficacy of the proposed method, its robustness in the presence of measuring errors, and show that the use of the signal phase leads to the best damage parameter estimation. Copyright © 2008 John Wiley & Sons, Ltd.

KEY WORDS: Hilbert transform; analytical signal; damage identification; measuring errors

1. INTRODUCTION

Damage can occur in structures during their service life due to extreme events and/or aggressive environmental conditions. In general, it manifests itself in a reduction of structural stiffness, leading to a loss of durability and safety conditions. For civil engineering it becomes of primary importance to detect and quantify damage at an early stage, much before structural collapse. In the past 40 years, many researchers have focused on this problem with the aim of providing a

*Correspondence to: Antonina Pirrotta, Dipartimento di Ingegneria Strutturale e Geotecnica, Università degli Studi di Palermo, Viale delle Scienze, 90128-Palermo, Italy.
†E-mail: pirrotta@diseg.unipa.it

Contract/grant sponsor: M.I.U.R; contract/grant number: 2004081204_005

Received 11 January 2007
Revised 18 December 2007
Accepted 21 January 2008

reliable damage identification procedure or a structural health monitoring program. Most of non-destructive techniques are based on the correlation between measured data (in the majority of cases from dynamic tests) and the response of an analytical model of the damaged structure (model-based procedures). Different structural response characteristics can be used for this purpose including modal data [1–4], curvature measures [5–7], frequency response functions (FRFs) [8–11] and strain energy [12–14]. However, the main issue of any identification procedure is damage sensitivity. A robust technique should be able to detect damage at very low level and in the presence of measuring noise; engineers need tools to recognize when dangerous situations may be initiated and well hidden behind an apparent structural integrity condition, avoiding the use of any complex algorithm. Frequency-based identification procedures often fail to give a satisfactory answer to this problem.

Analyses based on the use of the Hilbert transform (HT) have been proposed for detecting and quantifying non-linearities. In [15, 16] the analysis is carried out in the frequency domain, using differences between HT and FRFs to detect system non-linearities, while in [17, 18] the authors use the properties of the analytical signal for the system characterization. Since the HT appears to be particularly effective in detecting system non-linearities, it has also been used for damage identification problems assuming non-linear damage models [19, 20] (breathing cracks), while in [21–24] HT is combined with a proper mode decomposition algorithm to solve an identification benchmark test on a linear structure.

The aim of this work is to show the potentiality of applying HT to detect and quantify damage at an early stage in linear systems; it is worth stressing that in this paper we deal with damage that causes loss of stiffness in some point of the structure. The HT tool is used to obtain the analytical representation of the system response. Then, a damage identification procedure based on an adimensional functional of the square of the difference between theoretical and measured data is proposed. The lowest value of the functional gives the damage parameter of the system. Specifically, attention is focused on the signal phase, and instantaneous frequency, since it will be shown that even low damage levels lead to considerable response variations between undamaged and damaged case. In order to assess the robustness of the proposed identification procedure, numerical applications on single degree of freedom (SDOF) and 3 degrees of freedom (3DOF) are presented using data records perturbed by measuring noise.

2. HT AND ANALYTICAL SIGNALS

Let $x(t)$ denote the response of a linear system. Its HT is defined as

$$\hat{x}(t) = \frac{1}{\pi}\mathscr{P}\int_{-\infty}^{\infty}\frac{x(\tau)}{t-\tau}\,\mathrm{d}\tau \tag{1}$$

where $\mathscr{P}$ stands for principal value; it is an integral transform of the original signal $x(t)$ with the kernel $1/\pi t$.

The complex signal

$$z(t) = x(t) + \mathrm{i}\hat{x}(t) \tag{2}$$

where i is the imaginary unit is called the *analytical signal* (see [15] for further reference). The latter can be interpreted as a rotating vector in a complex plane; indeed, rewriting $z(t)$

DOI: 10.1002/stc

in the form

$$z(t) = A(t)\exp[\mathrm{i}\vartheta(t)] \tag{3}$$

$A(t)$ is the so-called *amplitude* (or envelope) of the rotating vector and $\vartheta(t)$ is the *phase angle*, respectively, defined as

$$A(t) = \sqrt{x(t)^2 + \hat{x}(t)^2}$$
$$\vartheta(t) = \arctan\left[\frac{\hat{x}(t)}{x(t)}\right] \tag{4}$$

The phase angle $\vartheta(t)$ is a function that lies in the interval $(-\pi,\pi)$, exhibiting jumps of 2π. In order to handle with a smooth function, it is convenient to use an unwrapping algorithm that corrects the radian phase angles by adding multiples of $\pm 2\pi$ when a jump occurs. In such a way the function $\vartheta(t)$ unwrapped is defined in the whole real set.

The time derivative of the analytical signal $\dot{z}(t)$ is also a complex signal related to $z(t)$ by

$$\dot{z}(t) = \dot{A}(t)\ \exp[\mathrm{i}\vartheta(t)] + \mathrm{i}\dot{\vartheta}(t)A(t)\ \exp[\mathrm{i}\vartheta(t)]$$
$$= \omega(t)z(t) \tag{5}$$

In Equation (5), $\omega(t)$ is a complex frequency defined as

$$\omega(t) = \frac{\dot{A}(t)}{A(t)} + \mathrm{i}\dot{\vartheta}(t) \tag{6}$$

The imaginary part of this vector $\dot{\vartheta}(t)$ represents the angular velocity of $z(t)$ in the $[x(t), \hat{x}(t)]$ plane, and it is referred to as *instantaneous frequency*. The reason for this is straightforward; for instance, if one assumes the original signal to be a cosinusoidal one, i.e. $x(t) = A\ \cos(\omega t)$, the analytical signal is a complex exponential $z(t) = A\exp(\mathrm{i}\omega t)$, where $A(t) = A$ and $\vartheta(t) = \omega t$. Thus, in this case, the instantaneous frequency coincides with the original circular frequency. In order to better clarify these concepts, the signal $x(t) = \cos(\omega t)$, its HT $\hat{x}(t) = \sin(\omega t)$, the phase $\vartheta(t)$ and the phase unwrapped are depicted in Figure 1.

3. DAMAGE SENSITIVITY

The main issue of any damage identification procedure is damage sensitivity. Often, the comparison between the response of the damaged and undamaged system does not provide any clue for recognizing a possible damage scenario. To show this, let us consider a massless cantilever bar with a pointmass m attached at its free end (Figure 2). The bar stiffness is EA/ℓ, its length being denoted by ℓ. Damage is modeled by a little reduction the axial stiffness $\mathrm{EA}(1-\alpha)/\ell$, where $\alpha \in [0, 1)$ is referred to as the damage coefficient. Although simple, this example is physically meaningful to our purpose and gives the possibility to trace some first heuristic consideration on the damage sensitivity of the signal features.

The equation governing the vibration of the given system under an impulsive force in horizontal direction $F(t) = \delta(t)$ (where $\delta(t)$ is Dirac's delta function) is

$$\ddot{x}(t) + 2\Lambda\dot{x}(t) + \omega_0^2(1-\alpha)x(t) = \delta(t)/m \tag{7}$$

where $\Lambda = \zeta_0\omega_0\sqrt{1-\alpha}$ denotes the damping term, ζ_0 the damping ratio and $\omega_0 = \sqrt{\mathrm{EA}/m\ell}$ is the undamaged bar circular frequency.

DOI: 10.1002/stc

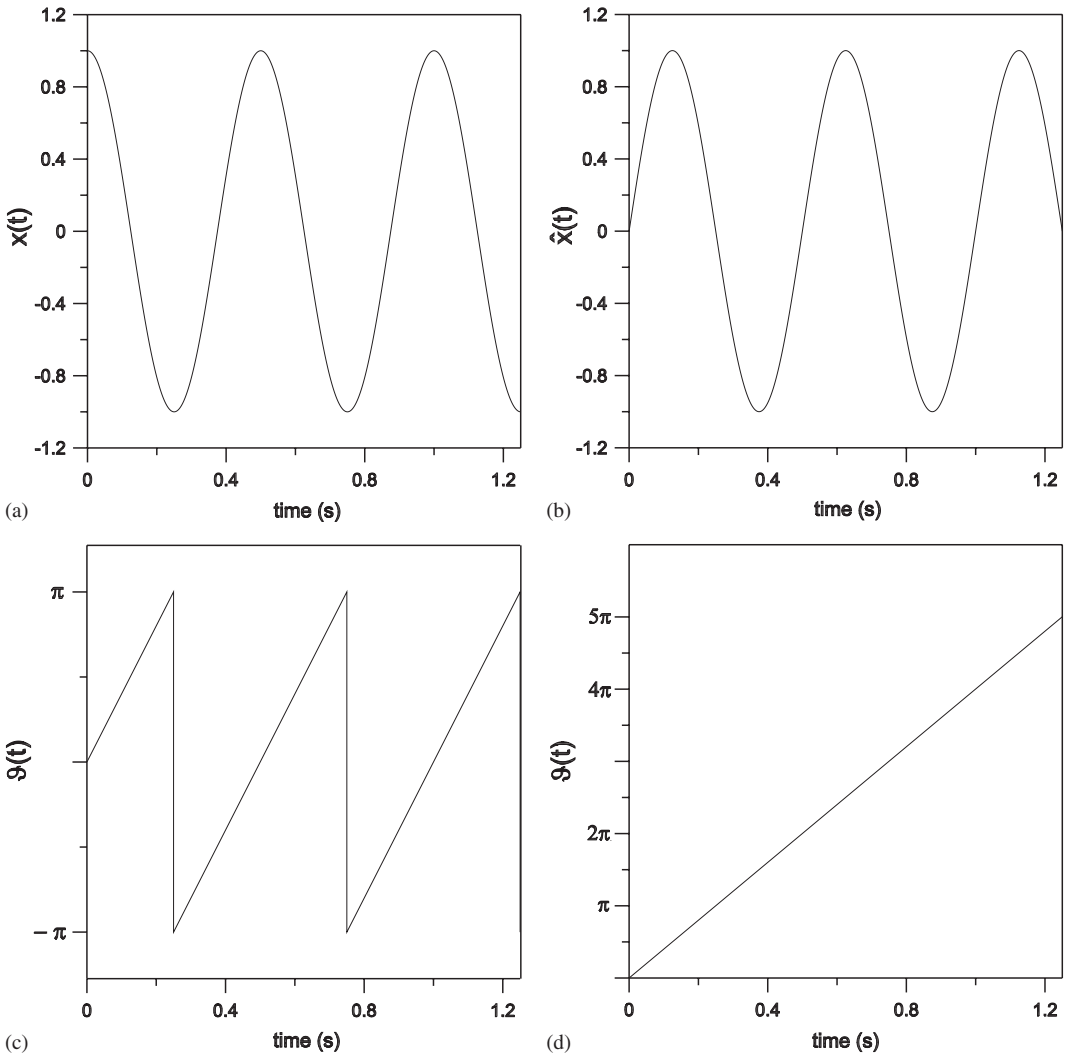

Figure 1. Example of the analytical features of the cosinusoidal signal: (a) original signal; (b) Hilbert transform of the signal; (c) phase; and (d) phase unwrapped.

In Figure 3 the impulse response function (IRF) and the FRF of the undamaged and damaged bar are reported. The damping ratio is assumed such that $\zeta_0\omega_0 = 1$ and the undamaged circular frequency is $\omega_0 = 10$ rad/s, while the damage coefficient is $\alpha = 0.01$ labeled as α_{eff}. The reduction in the system frequency from the undamaged to the damaged case is just of 0.59%; thus, a small damage scenario is analyzed in fact in Figure 3; the response of the damaged system totally overlaps the response of the undamaged one in both domains, and then it is not possible to predict this kind of damage. Our purpose is to look for a system feature that is sensitive to detect little damage. To aim at this we have to consider the characteristics of the analytical signal calculated on the IRF.

DOI: 10.1002/stc

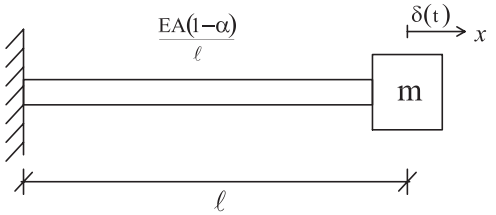

Figure 2. Massless cantilever bar of length ℓ with a point mass m.

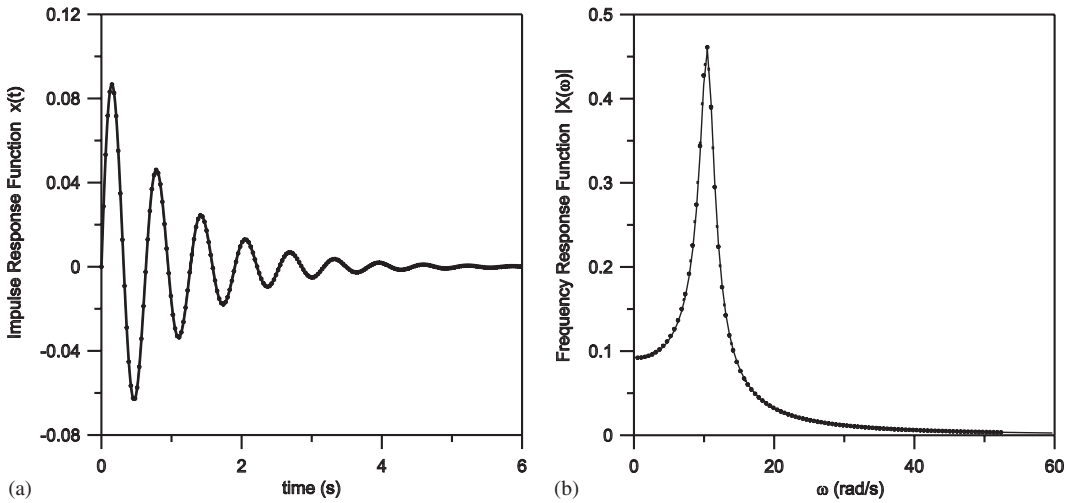

Figure 3. Comparison between undamaged (solid) and damaged (dotted) system response: (a) impulse response function and (b) frequency response function.

By applying the HT to the undamaged and damaged IRF, it is possible to construct the corresponding analytical signals. In Figure 4 the two signals are compared in a polar plot at different time instants. It can be noted that the amplitude of the damaged structure IRF is practically the same to the amplitude of the sound structure IRF. That is, low levels of damage do not produce high variations in the amplitude of the analytical signal. In this sense, we say that the amplitude is not a 'good feature' in the damage identification procedure. On the contrary, a clear and identifiable phase shift between the two vectors is evident. From this heuristic analysis, the phase seems to be more detectable and, consequently, more suited to highlight even *ab initio* damage scenario in the structure. In this contest we can say that the phase is a 'good feature' in damage identification. In the following, we will quantify the behavior of these features in relation to the procedure proposed.

4. DAMAGE IDENTIFICATION PROCEDURE

The idea is to define a functional highlighting the difference between the *experimentally measured* system response and the same response computable from an appropriate model of the system, referred to as the *theoretical system response*. The more the model approximates the

DOI: 10.1002/stc

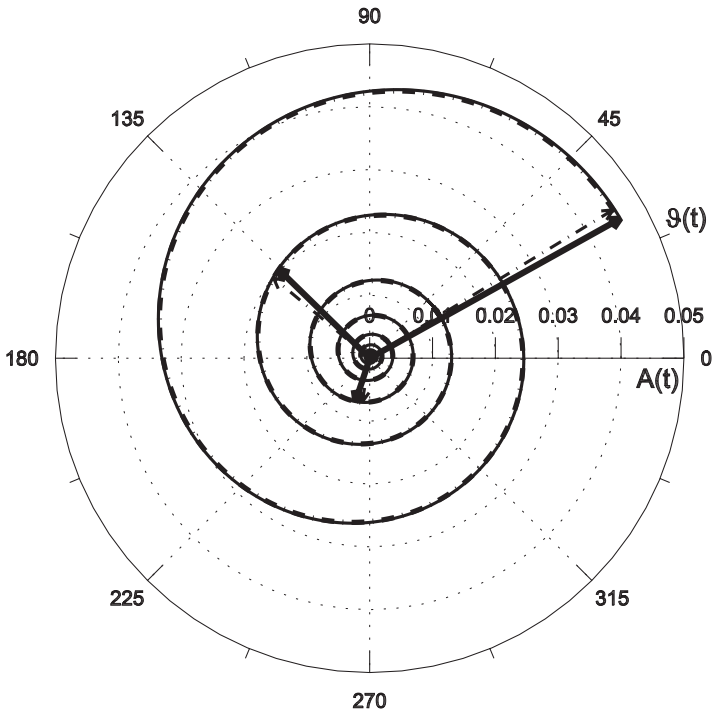

Figure 4. Polar plot of the analytical signal at multiple times ($T_0 = 2\pi/\omega_0$): undamaged (thicker solid) and damaged (thinner dashed).

damaged system under the experiment, the more this difference tends to zero. Thus, if the functional is properly defined as a function of the damage parameter, it will be possible to identify the state of the system by this comparison. The challenge for defining such an objective function is not easy for many reasons. It must be simple to compute, and it should not be sensible to data error, i.e. coming from ambient or instrumental noise. Moreover, it should be required that the damage-based objective function does not have an oscillatory behavior with local minima. We propose the following adimensional objective function to detect damage at early stage, defined as

$$J_\eta(\alpha) = \frac{\int_{T_i}^{T_f} (\eta^{\text{th}}(\alpha, t) - \eta^{\text{ex}}(\alpha_{\text{eff}}, t))^2 \, \mathrm{d}t}{\int_{T_i}^{T_f} \eta^{\text{ex}}(\alpha_{\text{eff}}, t)^2 \, \mathrm{d}t} \tag{8}$$

where $[T_i, T_f]$ is the observation window, $\eta(t)$ is a general feature of the system response (time history displacement, or velocity, acceleration, or amplitude, phase, instantaneous frequency calculated from the displacement or velocity or acceleration), while the apexes th and ex stand for theoretically determined, varying the value of α, and experimentally measured, or numerically simulated, affected by α_{eff}, respectively. Although the analytical signal and the original signal contain the same information, the behavior of functional (8), defined on the amplitude $A(t)$, the phase $\vartheta(t)$, the instantaneous frequency $\dot{\vartheta}(t)$ or the displacements of the system is clearly different. From the above considerations we expect that the phase is a system

DOI: 10.1002/stc

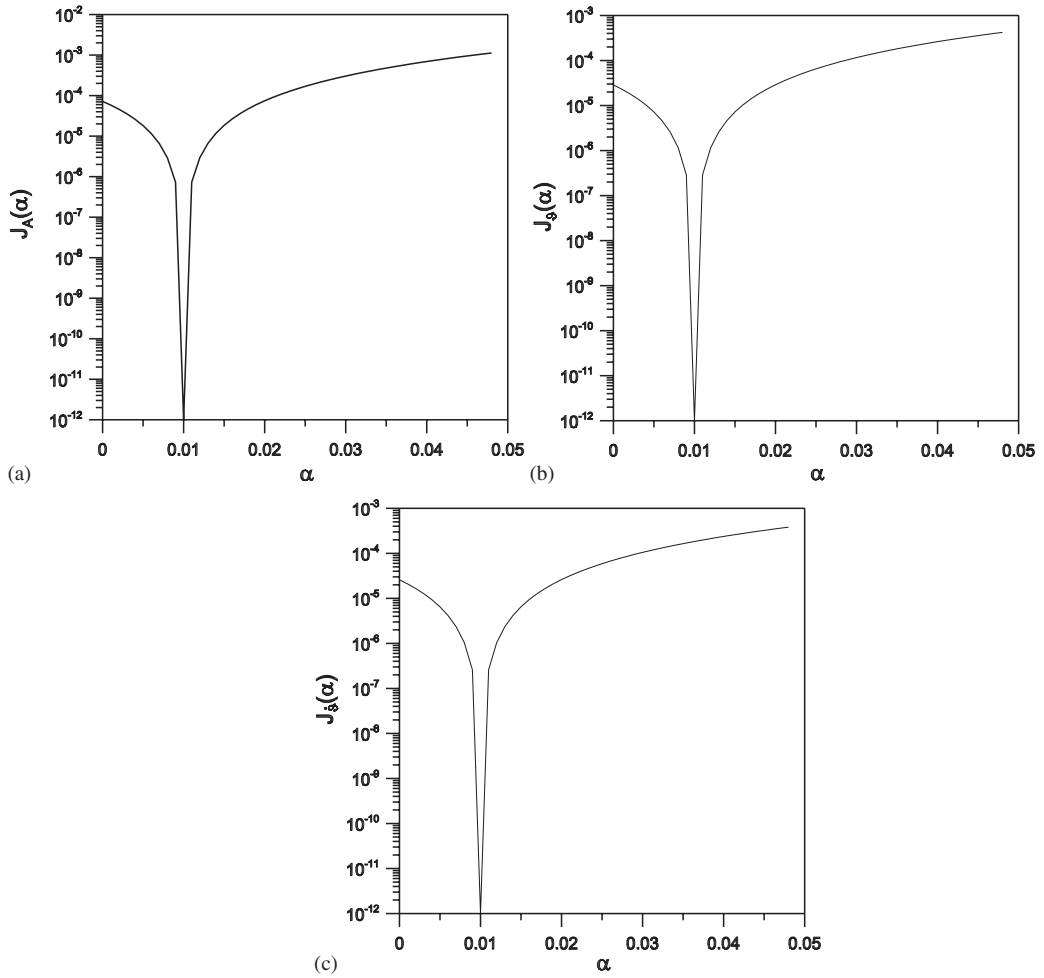

Figure 5. Variation of the objective function *versus* α for a simulated impact hammer test: (a) amplitude; (b) phase; and (c) instantaneous frequency.

feature better than others to highlight little changes in stiffness of the system, that is, functional (8) based on this feature should have better performance. This will be proved in the following by means of some benchmark-simulated test.

4.1. Simulated impact hammer test

Let us assume that impact hammer test data are available for the SDOF structure, whose mechanical and damage parameters are those reported in Section 3, and let the observation window time be $T_i = 0$ s, $T_f = 6$ s.

First, the experimental displacement of the damaged system $x^{\mathrm{ex}}(\alpha_{\mathrm{eff}}, t)$ is simulated, and the analytical signal is calculated by means of numerical HT; then, varying α in the range [0,1) with steps of $\Delta\alpha = 0.001$, the function response in terms of displacements $x^{\mathrm{th}}(\alpha, t)$, amplitude $A^{\mathrm{th}}(\alpha, t)$,

DOI: 10.1002/stc

phase $\vartheta^{\text{th}}(\alpha, t)$ and instantaneous frequency $\dot{\vartheta}^{\text{th}}(\alpha, t)$ are evaluated, and finally the integral (8) is calculated for each feature considered. Results are reported in Figure 5. The lowest value of the objective function defined $J_\eta(\alpha)$ is localized at $\alpha = 0.01$ in each case and it identifies the damage level of the structure. In order to highlight this value, a logarithmic scale has been used for the y-axis; thus, in each of Figure 5 a sharp peak is obtained.

The heuristic considerations on the goodness of the objective functions in the previous section can now be quantified in terms of performance of the minimization algorithm applied to the functional of the acceleration $J_{\ddot{x}}(\alpha)$, of the amplitude $J_A(\alpha)$, of the phase $J_\vartheta(\alpha)$ and of the instantaneous frequency $J_{\dot{\vartheta}}(\alpha)$. To aim at this, Mathematica© built-in minimization subroutines based on Newton and quasi-Newton minimization methods have been used. While the Newton algorithm is based on the computation of the first and second derivatives of the objective function [25], in the quasi-Newton method the second-order derivative is approximated with the Broyden–Fletcher–Goldfarb–Shanno method, described in [26]. Of course, differences in terms of computational time between the two algorithms become important when more damaged parameters are considered, although being indicative in this simple scalar case. In Table I the performance of the algorithms used is summed up by means of four categories: the value of the identified damage, the number of steps needed to reach the assigned tolerance, the number of evaluation points of the objective function and the computational time expressed in seconds (central processing unit; CPU time). The number of evaluations and the CPU time in the case of the phase-based and instantaneous frequency-based objective functions are less than others, and therefore phase and instantaneous frequencies are preferable. In this contest, we could say that the latter features are more sensitive with respect to the minimization procedure. It is clear that computational effectiveness of the functionals is striking in multiple degrees of freedom (MDOF) structures with more damaged parts and, then, short computational time is preferred. We will show in the next sections that, among the analytical features, the phase is also the most reliable for robustness' sake with respect to signal with measurement noise.

5. IDENTIFICATION PROCEDURE IN THE PRESENCE OF MEASUREMENT NOISE

In this section, in order to assess the robustness of the proposed identification procedure, simulated records are affected by a random noise, $W(t)$. The noise, superimposed to all simulated recorded data, is a band-limited Gaussian noise with standard deviation equal to 10% of a third of the maximum peak of acceleration response. In Figure 6(a) the displacement time

Table I. Performance of the functionals calculated on the signal without noise: functional J, value of the identified damage, the number of steps needed, the number of evaluation points of J and computational time expressed in seconds (CPU time).

Newton method					Quasi-Newton method				
J	α	# Steps	# Eval.	CPU(s)	J	α	# Steps	# Eval.	CPU(s)
$J_{\ddot{x}}(\alpha)$	0.010	3	4	0.031	$J_{\ddot{x}}(\alpha)$	0.010	4	6	0.047
$J_A(\alpha)$	0.010	3	4	0.016	$J_A(\alpha)$	0.010	4	5	0.047
$J_\vartheta(\alpha)$	0.010	2	3	<0.001	$J_\vartheta(\alpha)$	0.010	4	5	<0.001
$J_{\dot{\vartheta}}(\alpha)$	0.010	2	3	<0.001	$J_{\dot{\vartheta}}(\alpha)$	0.010	4	5	<0.001

DOI: 10.1002/stc

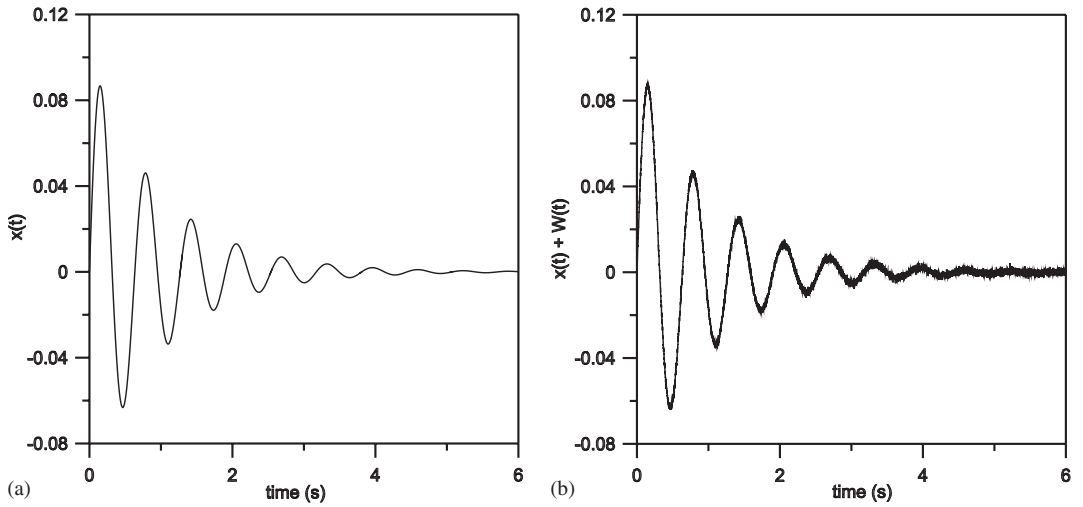

Figure 6. Displacements of the SDOF: (a) without noise and (b) with measurement noise.

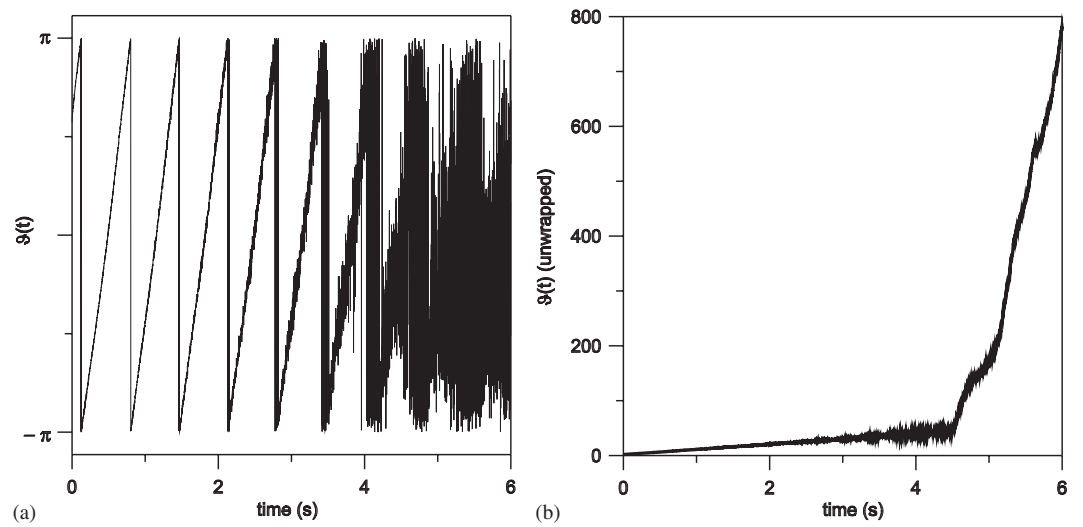

Figure 7. Signal with measurement noise: (a) phase with noise and (b) phase unwrapped with noise.

history $x(\alpha_{\text{eff}}, t)$ of the damaged system is depicted, and in Figure 6(b) the same signal affected by noise measurements, $x(\alpha_{\text{eff}}, t) + W(t)$, is reported. Taking into account the measurement noise, the extension of the aforementioned damage identification procedure is not straightforward because the results by using Equation (8) are not satisfactory as the previous case. In fact, depending on the parameter of the system and the level of the noise, the signal is mixed up with the noise in the last instants of the time window $[T_i, T_f]$, as the signal decays. For example, considering the displacement of the damaged structure recorded in the presence of noise, labeled $x(\alpha_{\text{eff}}, t) + W(t)$, the phase $\vartheta(t)$ of its analytical signal is plotted in Figure 7(a); after $t \cong 4$ s the record is highly affected by the noise. Further, the unwrapping algorithm, needed to take into

DOI: 10.1002/stc

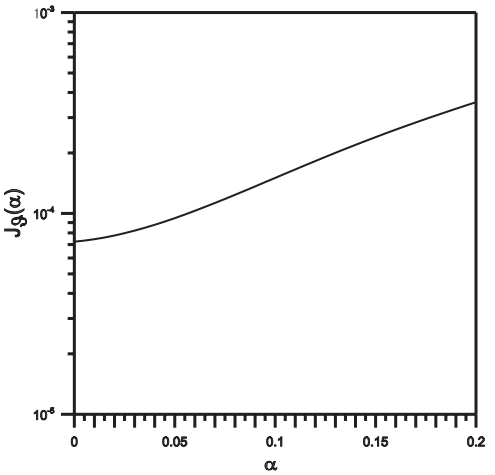

Figure 8. Objective function calculated on the phase (unwrapped) of the displacement affected by measurement noise.

account the cycles that the vector produces in the complex plane, returns a phase that rears up in the last few seconds (Figure 7(b)), compromising the robustness of the method.

Functional (8) can be explicitly expressed as

$$J_\vartheta(\alpha) = \frac{\int_{T_i}^{T_f} (\vartheta^{\text{th}}(\alpha, t) - \vartheta^{\text{ex}}(\alpha_{\text{eff}}, t, W(t)))^2 \, \mathrm{d}t}{\int_{T_i}^{T_f} (\vartheta^{\text{ex}}(\alpha_{\text{eff}}, t, W(t)))^2 \, \mathrm{d}t} \tag{9}$$

and it is plotted in Figure 8, where the y-axis is in the logarithmic scale. The presence of the measurement noise does not induce in functional (9) a sharpened peak and the minimization procedure may not converge. This happens because the analyzed signal does not have a well-behaved HT. Then, it needs a proper procedure to restore the validity of the method.

5.1. *Use of a filter to restore the procedure efficiency*

In order to restore the validity of the identification procedure described above, it is necessary to filter the recorded signal. There are many kinds of filters in literature: Butterworth, Elliptic or Chebyshev of the first and second kind and so on, with different specifications [27]. Our aim is to have the minimum distortion of the filtered signal and to cut the highest noise frequencies above a certain value that is commonly called cutoff frequency. Butterworth low-pass filter has these characteristics and therefore seems to be the best option. The behavior of such a filter can be summarized by the so-called FRF $H(s)$, with s being a complex number, which has the following form:

$$H(s) = \frac{\Omega_C^N}{\prod_{k=1}^{N} (s - p_k)} \tag{10}$$

where Ω_C is the cutoff frequency (rad/s), N is the order of the filter

$$p_k = \Omega_c \ \exp\left[\mathrm{i}\left(\frac{\pi}{2} + \frac{\pi}{2N}(2k-1)\right)\right]$$

DOI: 10.1002/stc

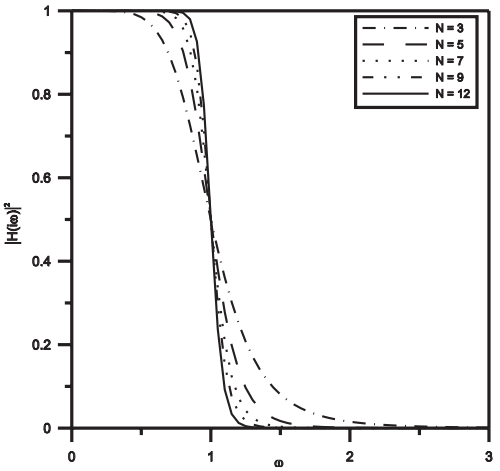

Figure 9. Butterworth low-pass filter: magnitude-squared function $\left|H(\mathrm{i}\omega)\right|^2$ for different filter orders.

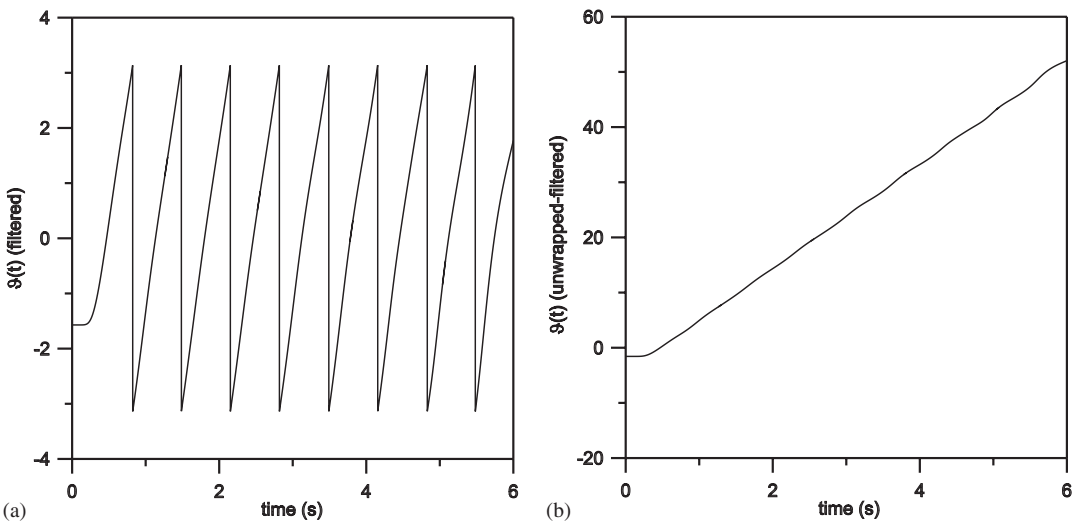

Figure 10. Filtered signal with measurement noise: (a) phase and (b) phase unwrapped.

are the poles (the roots of the denominator) and $\mathrm{i} = \sqrt{-1}$ is the imaginary unit. From definition (10) with the position $s = \mathrm{i}\omega$, the so-called gain function or magnitude-squared function $\left|H(\mathrm{i}\omega)\right|^2$ is obtained. When $\omega = 0$, $\left|H(\mathrm{i}\omega)\right|^2 \to 1$ and the frequency component will be completely passed. When $\omega \to \infty$, the magnitude-squared function $\left|H(\mathrm{i}\omega)\right|^2 \to 0$ and the frequency components are completely stopped. Between the pass band and the stop band, there is a transition band ($0 < H(\mathrm{i}\omega) < 1$) in which the frequency component will be partially passed. When $\omega = \Omega_c$, $\left|H(\mathrm{i}\omega)\right|^2$ always becomes 0.5 (half power) regardless of the order of the filter N.

In Figure 9 the effects of the filter order N on the frequency response are shown for a Butterworth low-pass filter with unitary cutoff frequency. If the filter order increases, the transition from the pass band to the stop band gets steeper.

DOI: 10.1002/stc

Moreover, converting a product into a sum:

$$\prod_{k=1}^{N}(s-p_k)=\sum_{k=0}^{N}c_k s^k \tag{11}$$

one can identify the coefficient c_k. Calling $x(t)$ and $y(t)$ the input signal and the output of the filter, respectively, and with $X(s)$ and $Y(s)$ their Laplace transform, the linear input–output relationship in Laplace space can be expressed as

$$Y(s)=H(s)X(s)=\frac{\Omega_C^N}{\sum_{k=0}^{N}c_k s^k}X(s) \tag{12}$$

that is

$$Y(s)\sum_{k=0}^{N}c_k s^k=\Omega_C^N X(s) \tag{13}$$

Then, the inverse Laplace transform gives the differential form of the filter that will be used to clean the signal from the noise:

$$\sum_{k=0}^{N}c_k\frac{\mathrm{d}^k}{\mathrm{d}t^k}y(t)=\Omega_C^N x(t) \tag{14}$$

In passing from Equation (13) to Equation (14), a general property of the Laplace transform has been taken into account:

$$\frac{\mathrm{d}^k}{\mathrm{d}t^k}y(t)=L^{-1}\left(Y(s)s^k-\sum_{r=0}^{k-1}s^r\frac{\mathrm{d}^{k-1-r}}{\mathrm{d}t^{k-1-r}}y(0)\right) \tag{15}$$

jointly to the assigned initial conditions:

$$y(0)=0$$

$$y'(0)=0$$

$$\ldots.$$

$$y^{(k-1)}(0)=0 \tag{16}$$

Equation (14) is a linear differential equation of order N that can be numerically solved and gives the output of the filter $y(t)$. Of course, following this procedure the input $x(t)$ and the output $y(t)$ of the filter are not in phase. Yet, a simple backward–foreward procedure (implemented in the Matlab© command *filtfilt*) gives back the two signals in phase. Therefore, in the following, the filtered signal will be always intended in phase with the input.

The displacements affected by the noise, $x(\alpha_{\mathrm{eff}}, t)+W(t)$, have been processed with a Butterworth filter with parameters $\Omega_C=\omega_0+15(\mathrm{rad/s})=25(\mathrm{rad/s})$ and $N=12$. After the application of the filter, the resulting signal $y(t)$ has a well-behaved HT: the phase assumes a regular behavior, as shown in Figure 10(a) and (b), and is now well suited for the procedure proposed through Equation (9). Then, the resulting time history output $y(t)$ has been considered for the evaluation of

DOI: 10.1002/stc

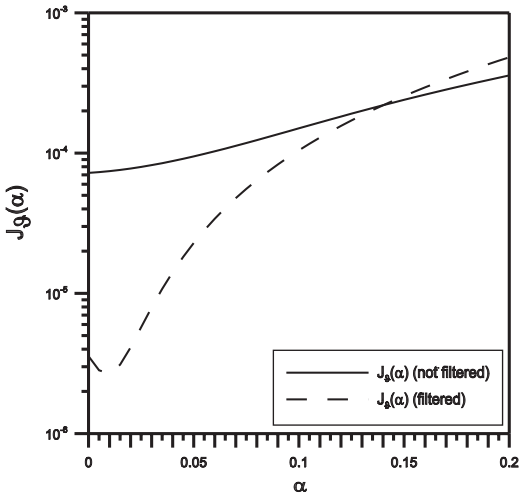

Figure 11. Objective function calculated on the phase (unwrapped): without filter (continuous line) and with filter (dashed line).

Table II. Performance of the functionals calculated on the signal with measurement noise: functional J, value of the identified damage, the number of steps needed, the number of evaluation points of J and computational time expressed in seconds (CPU time).

Newton method					Quasi-Newton method				
J	α	# Steps	# Eval.	CPU(s)	J	α	# Steps	# Eval.	CPU(s)
$J_{\bar{x}}(\alpha)$	—	—	—	—	$J_{\bar{x}}(\alpha)$	—	—	—	—
$J_A(\alpha)$	—	—	—	—	$J_A(\alpha)$	—	—	—	—
$J_\vartheta(\alpha)$	0.013	2	3	0.031	$J_\vartheta(\alpha)$	0.013	4	5	0.031
$J_{\dot{\vartheta}}(\alpha)$	0.016	3	4	0.015	$J_{\dot{\vartheta}}(\alpha)$	0.016	4	5	0.031

the analytical signal. By adopting the same procedure as before, the validity of the damage identification is restored as shown in Figure 11, where the functional $J_\vartheta(\alpha)$ calculated from the filtered displacement shows a well-marked peak (dashed line) corresponding to the damage value.

In Table II, results on the sensitivity of the objective functions are reported. Both the Newton and the quasi-Newton methods did not converge to a solution in case of functional based on the displacements and on the amplitudes, while the identified damage was $\alpha = 0.013$ and 0.016 having used the phase and the instantaneous frequency, respectively. That is, the phase of the analytical signal is more sensitive than other features not only from a computational perspective, but also with respect to the precision of the identified damage coefficient, even in the presence of measurement noise. For these reasons, in the following extension to MDOF structures, we will refer to just the objective function based on the phase.

6. EXTENSION TO MDOF SYSTEMS

The extension to MDOF systems is not straightforward because the proposed method by using Equation (8) is not satisfactory as the case of SDOF, depending strongly on the structural

DOI: 10.1002/stc

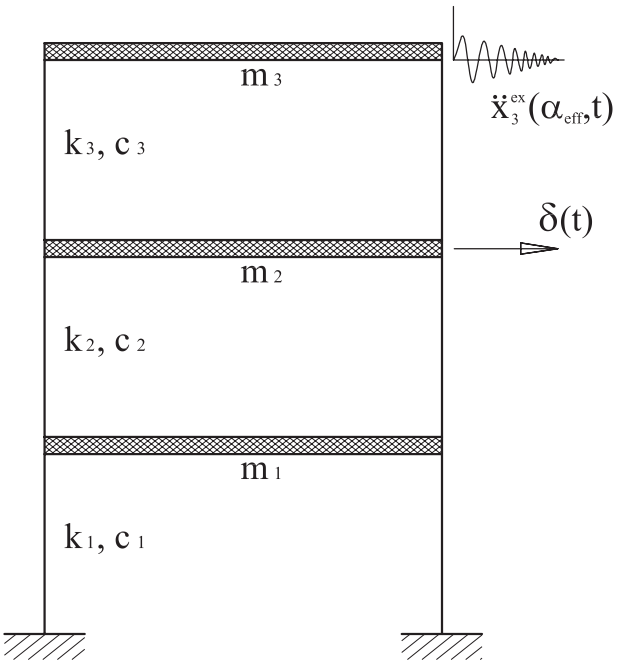

Figure 12. Three shear-beam building model.

parameters. In this section, by resorting to a numerical application, the physical reason of this ill-posed problem will be shown. In the next section, by means of a filtering technique, the validity of the procedure on the analytical signal will be restored. Let us consider a three-storey shear-beam-type building analyzed in [24] and depicted in Figure 12. The mass, stiffness and viscous damping of each storey are assumed to be the same, with $m_j = 1000\,\text{kg}$, $k_j = 980\,\text{KN/m}$, $c_j = 2814\,\text{Ns/m}$, respectively, for $j = 1, 2, 3$. Damage is simulated by decreasing the stiffness at the first floor by a damage coefficient α_{eff} chosen as $\alpha_{\text{eff}} = 0.01$, that is, we consider a global damage coefficient.

Suppose an impact loading is applied to the second floor; the simulated time history acceleration response, for instance, at the third floor $\ddot{x}_3^{\text{ex}}(\alpha_{\text{eff}}, t)$ and the correspondent Fourier spectrum are calculated and depicted in Figure 13. By looking at a Fourier spectrum of the damaged system response $\ddot{x}_3^{\text{ex}}(\alpha_{\text{eff}}, t)$ (Figure 13(b)), it appears that the second and the third modes do not contribute strongly. A measurement noise, as previously done, is superimposed to the simulated acceleration $\ddot{x}_3^{\text{ex}}(\alpha_{\text{eff}}, t)$, and it strongly affects both the acceleration and the spectrum (Figure 13(c)–(d)). The analysis previously described is then performed and the functional of the phase is reported, because it is the most significant as in the SDOF system. To aim at this, the functional $J_\vartheta(\alpha)$ in Equation (9) is calculated once the analytical signal of both $\ddot{x}_3^{\text{ex}}(\alpha_{\text{eff}}, t)$ and $\ddot{x}_3^{\text{th}}(\alpha, t)$ and the correspondent phases have been evaluated, where α assumes values in the range (0,0.8) with step $\Delta\alpha = 0.001$. In Figure 14 it is shown that the aforementioned method is efficient in detecting damage, but the presence of local minima in $J_\vartheta(\alpha)$ (highlighted with dotted circles in the figure) could affect the identification procedure.

DOI: 10.1002/stc

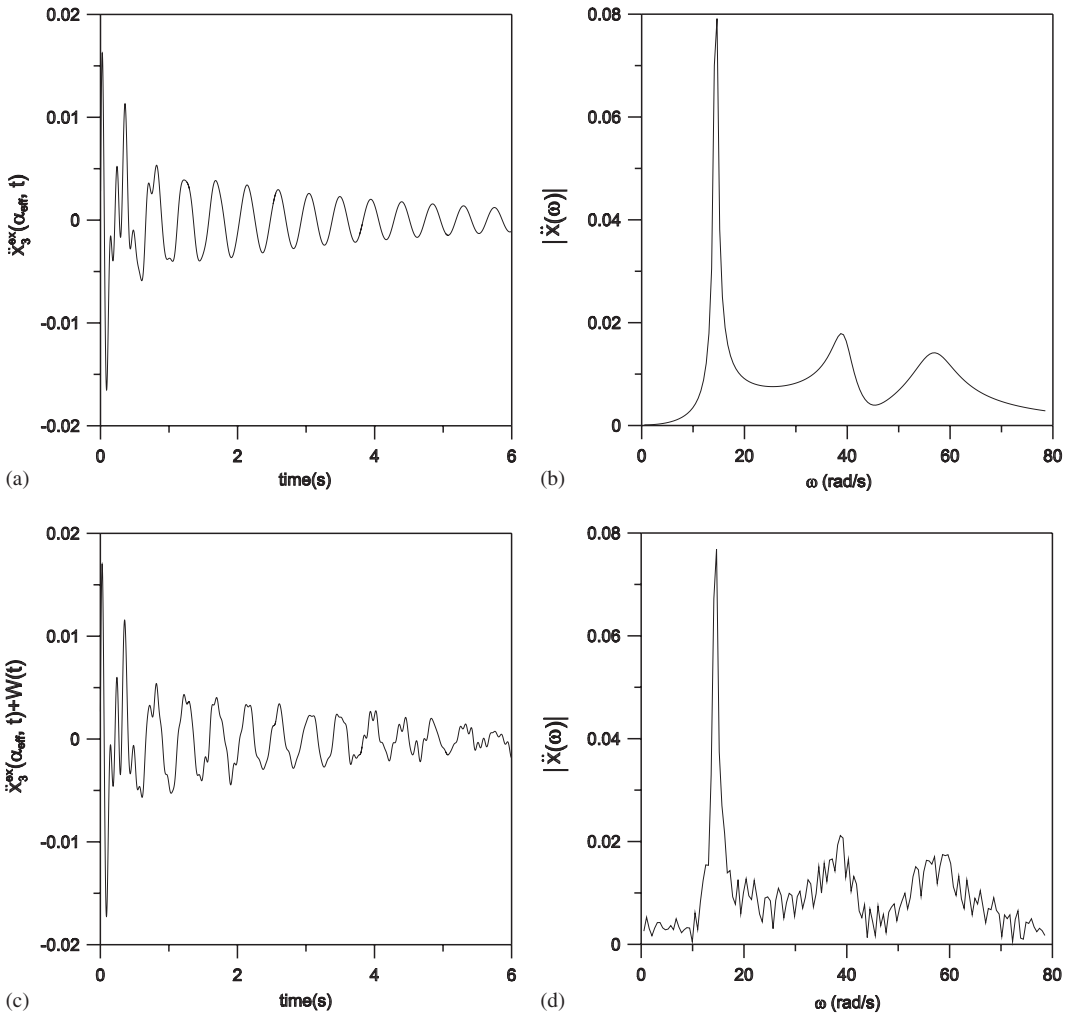

Figure 13. Simulated response of the third floor: (a) acceleration of the third floor $\ddot{x}_3^{\mathrm{ex}}(\alpha_{\mathrm{eff}}, t)$; (b) Fourier spectrum of $\ddot{x}_3^{\mathrm{ex}}(\alpha_{\mathrm{eff}}, t)$; (c) acceleration of the third floor with noise: $\ddot{x}_3^{\mathrm{ex}}(\alpha_{\mathrm{eff}}, t) + W(t)$; and (d) Fourier spectrum of $\ddot{x}_3^{\mathrm{ex}}(\alpha_{\mathrm{eff}}, t) + W(t)$.

This happens because the HT allows the damage identification only if the analyzed signal is monocomponent or almost monocomponent, i.e. what we have already indicated as well-behaved HT of the signal. Therefore, it needs a monocomponent signal to restore the validity of the method; this can be achieved, for example, by use of Hilbert Huang algorithm [21–24], labeled empirical mode decomposition that, in fact, separates the multicomponent signal in a summation of the so-called intrinsic mode functions. The only problem is that this technique is based on empirical observations, i.e. no analytical tools may be used. In the next section, we propose a different way to reduce the signals in monocomponent ones, resorting to the filtering technique. That is, when MDOF systems are considered, band-pass filtering has the double effect: (i) to reduce the influence of the

DOI: 10.1002/stc

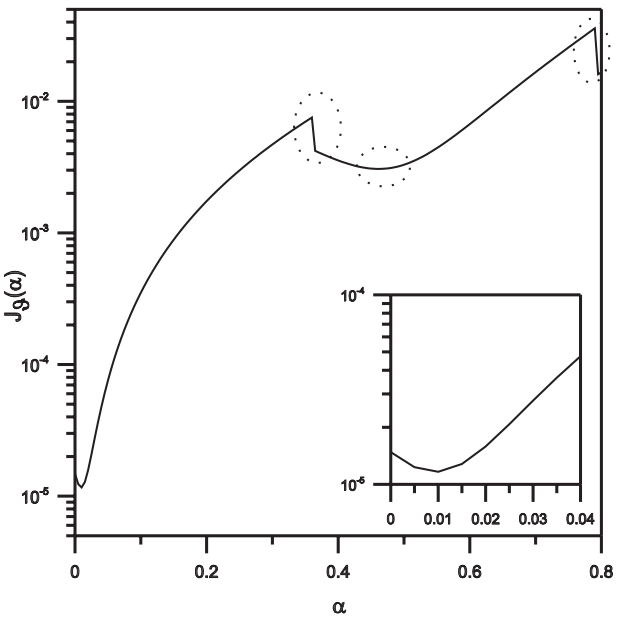

Figure 14. Objective function in terms of phase (unwrapped) *versus* α for the 3DOF system, in the presence of measurement noise; below, a zoom in the neighborhood of $\alpha_{\text{eff}} = 0.01$.

measurement noise and (ii) to separate each modal response, giving the searched signal with well-behaved HT. The identification procedure will be based on the analytical signal of one of the modal structural response.

7. EXTRACTING THE MODAL RESPONSES TO RESTORE THE PROCEDURE VALIDITY

As is well known, from the modal analysis, the response of an n-degree of freedom system is the sum of the modal responses $\ddot{x}_{pj}(t)$

$$\ddot{x}_p(t) = \sum_{j=1}^{n} \ddot{x}_{pj}(t) = \sum_{j=1}^{n} \phi_{pj}\ddot{q}_j(t) \tag{17}$$

where ϕ_{pj} is the pj element of the system modal matrix and $q(t)$ the displacement in the modal space.

Thus, it occurs to extract from the acceleration response the modal responses $\ddot{x}_{pj}(t)$, for each mode j, using several low-pass filters of the same kind as those in Section 5.1.

Once selected the parameters characterizing the low-pass filters, the procedure to extract the modal responses is summarized as follows:

1. First a Fourier spectrum of the damaged system acceleration response is performed, such that one can determine not only the natural frequencies of the system, but also the

DOI: 10.1002/stc

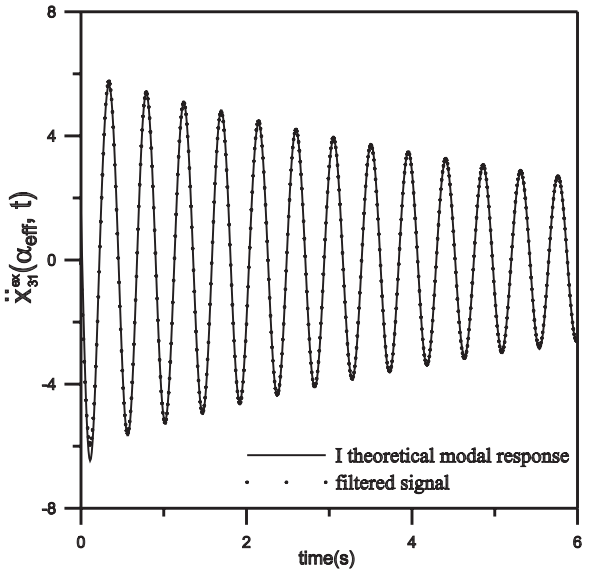

Figure 15. Comparison between the first theoretical modal response of the system (continuous line) and the signal obtained by filtering the response (dotted line).

approximate frequency range around each natural frequency ω_j, say

$$\omega_{jL} < \omega_j < \omega_{jH} \tag{18}$$

2. then low-pass filters are applied twice for each natural frequency having as Ω_C the cutoff frequency ω_{jL} and ω_{jH}, respectively;
3. finally, the difference between the time histories' output solution of the equation of the filter in differential form (Equation (14)) with $\Omega_C = \omega_{jH}$, and $\Omega_C = \omega_{jL}$, well approximate the modal response

$$\ddot{y}_{p,j} = [\ddot{y}_{p,\omega_{jH}}(t) - \ddot{y}_{p,\omega_{jL}}(t)] \approx \ddot{x}_{pj}(t) \tag{19}$$

In order to show how to use this procedure let us come back to the previous application. First of all, for the factorization of c_k, the poles (the roots of the denominator in Equation (10)) must be obtained. The filter order $N = 8$ leads to a good performance of the filter and avoids further complications, due to the increasing order of the differential equations, Equation (14). To extract the modal response from the signal, the aforementioned steps have to be followed. First of all, the natural frequencies have to be found. As reported in the Fourier spectrum of the damaged system response $\ddot{x}_3^{\text{ex}}(\alpha_{\text{eff}}, t)$, (Figure 13(d)) the three natural frequencies are $\omega_1 = 13.62$ rad/s (2.17 Hz); $\omega_2 = 38.48$ rad/s (6.12 Hz); $\omega_3 = 56.17$ rad/s (8.94 Hz). Thus, to determine the modal responses, using filtering, the following frequency ranges are selected:

(i) $0.82 \text{ rad/s} = \omega_{1L} < \omega_1 < \omega_{1H} = 25.9 \text{ rad/s}$ for the first mode;

DOI: 10.1002/stc

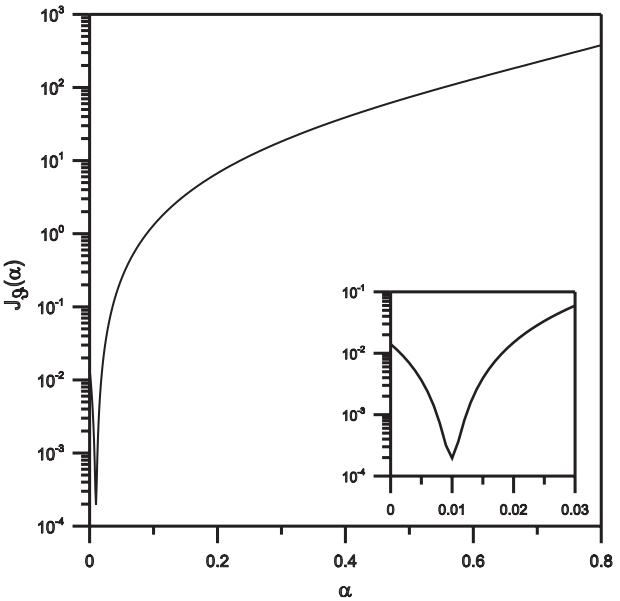

Figure 16. Objective function in terms of phase (unwrapped) of the first modal response extracted by the filter; below, a zoom in the neighborhood of $\alpha_{\text{eff}} = 0.01$.

(ii) 25.9 rad/s $= \omega_{2L} < \omega_2 < \omega_{2H} =$ 47.7 rad/s for the second mode;
(iii) 47.7 rad/s $= \omega_{3L} < \omega_3 < \omega_{3H} =$ 65.3 rad/s for the third mode.

For instance to find out the first modal response using the signal response at the third floor, it is necessary to process this signal $\ddot{x}_3^{\text{ex}}(\alpha_{\text{eff}}, t)$ depicted in Figure 13(c), through the eighth-order low-pass filter twice; first using the filter having $\Omega_C = \omega_{1H} = 25.9$ rad/s, then the filter having $\Omega_C = \omega_{1L} = 0.82$ rad/s. The resulting time history obtained by the difference between the time histories' output, solution of both the equations of the filters in differential form (Equation (14)) ($\ddot{y}_{3,1} = [\ddot{y}_{3,\omega_{1H}}(t) - \ddot{y}_{3,\omega_{1L}}(t)] \approx \ddot{x}_{31}(t)$), well approximates the first modal response, as reported in Figure 15. Analogously, we can extract the other modal responses by processing the signal $\ddot{x}_3^{\text{ex}}(\alpha_{\text{eff}}, t)$ with the eighth-order low-pass filter twice, for each mode, with a frequency band $\omega_{jL} < \omega_j < \omega_{jH}$ $(j = 1, 2, 3)$ given above. The resulting three-time histories obtained by the difference $\ddot{y}_{p,j} = [\ddot{y}_{p,\omega_{jH}}(t) - \ddot{y}_{p,\omega_{jL}}(t)] \approx \ddot{x}_{pj}(t)$ thus obtained well approximate each modal response. We label these functions $\ddot{x}_{pj}^{\text{ex}}(\alpha_{\text{eff}}, t)$, since they have been obtained for the damaged system.

So far we are in the same condition as the previous case: a signal that has a well-behaved HT. Thus, after considering the analytical signal of both the first modal responses $\ddot{x}_{31}^{\text{ex}}(\alpha_{\text{eff}}, t)$ extracted and $\ddot{x}_{31}^{\text{th}}(\alpha, t)$ (varying α), the functional $J_\vartheta(\alpha)$ based on the phase ϑ_{31} is calculated from Equation (8).

Results are depicted in logarithmic scale in Figure 16. By looking at this figure, it is evicted that the validity of the proposed method is restored being efficient in detecting damage again. The effect of the filter in this case, compared with the SDOF system, is double because it cuts

DOI: 10.1002/stc

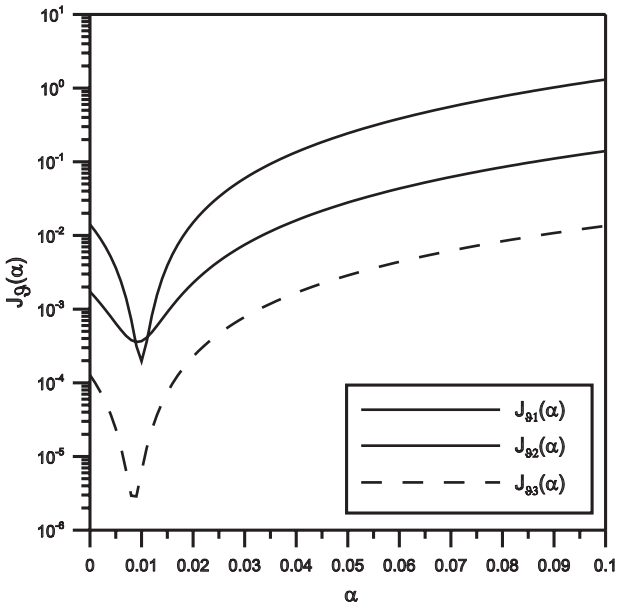

Figure 17. Objective function in terms of phase of the modal responses extracted from the recorded signal by a filter: $J_{\vartheta 1}(\alpha)$ from the first modal response; $J_{\vartheta 2}(\alpha)$ from the second modal response; and $J_{\vartheta 3}(\alpha)$ from the third modal response.

out: (i) the frequency content, due to the other modal components and (ii) the higher frequencies due to the band-limited Gaussian noise.

As observable from Figure 17, functionals $J_{\vartheta 2}(\alpha)$ and $J_{\vartheta 3}(\alpha)$, calculated from the second and the third modal responses, respectively, seem to be also suited for the identification of the damage level. The third modal response shows the worst behavior because it lasts just for a few instants and thus it is affected more than others by numerical error due to the filter dynamics or the numerical HT. Of course, the first modal response is the easiest to find because the filter can be applied only once; then we find it more convenient just to identify the damage with the phase of the first modal response of the structure. These results show that the procedure based on the phase is, in general, a robust way to detect the damage on real structures with real measurements. Experimental tests on a 2DOF shear-type model subjected to several damage scenarios have been analyzed in [28], and the obtained results show the effectiveness of the method in accordance with those obtained numerically.

8. CONCLUSIONS

In this paper the incipient damage identification problem has been investigated by using simulated data records in dynamic setting. Comparison of response variations due to damage in terms of amplitude, phase and instantaneous frequency has been made in order to assess the sensitivity of these response quantities to the parameter variations due to damage. The response quantities have been defined in the complex plane by introducing the so-called analytical signal, the imaginary part being the HT of the real part. It has been shown that, especially for small

DOI: 10.1002/stc

damage extent, the response in terms of IRF and amplitude is almost insensible to the system perturbation, which makes a damage identification based on this response characteristic unfeasible. Conversely the phase and the instantaneous frequency exhibit high sensitivity to stiffness changes, where the first is preferred to the latter. In conclusion to this study, the following remarks can be highlighted: (i) a damage identification procedure may be advantageously performed by using the phase; (ii) it has been shown that the method is reliable if one deals with monocomponent signal; (iii) the method proposed has been extended to multicomponent signals (such as the response to SDOF and MDOF structures affected by measurement noise) by an opportune Butterworth's filter preprocessing that gives back a monocomponent signal. In this paper, the damage identification procedure has been performed only by means of numerical tests.

ACKNOWLEDGEMENTS

This work is part of a larger national research project coordinated by Prof. L. Materazzi and supported by M.I.U.R through grant 2004–2006 prot. 2004081204_005. The financial support is gratefully acknowledged.

REFERENCES

1. Adams RD, Cawley P, Pye CJ, Stone BJ. A vibration technique for non-destructively assessing the integrity of structures. *Journal of Mechanical Engineering Science* 1991; **20**:93–100.
2. Davini C, Gatti F, Morassi A. A damage analysis of steelbeams. *Meccanica* 1992, **22**:321–332.
3. Gounaris GD, Papadopoulus CA, Dimarogonas AD. Crack identification in beams by coupled response measurements. *Computer and Structures* 1996; **58**:299–302.
4. Cerri MN, Vestroni F. Detection of damage in beams subjected to diffused cracking. *Journal of Sound and Vibration* 2000; **234**:259–276.
5. Pandey AK, Biswas M, Samman MM. Damage detection from changes in curvature mode shapes. *Journal of Sound and Vibration* 1991; **145**:321–332.
6. Luo H, Hanagud S. An integral equation for changes in the structural dynamics characteristics of damaged structures. *International Journal of Solids and Structures* 1997; **34**:4557–4579.
7. Ratcliffe CP. A frequency and curvature based experimental method for locating damage in structure. *Journal of Vibration Acoustics* 1999; **226**:1029–1042.
8. Wang Z, Lin RM, Lim MK. Structural damage detection using measured FRF data. *Computer Methods in Applied Mechanics* 1997; **147**:187–197.
9. Thyagarajan SK, Schulz MJ, Pai PF. Detecting structural damage using frequency response functions. *Journal of Sound and Vibration* 1998; **210**:162–170.
10. Sampaio RPC, Maia NMM, Silva JMM. Damage detection using frequency-response-function curvature method. *Journal of Sound and Vibration* 1999; **226**:1029–1042.
11. Lee U, Shin J. A frequency response function-based structural damage identification method. *Computer and Structures* 2002; **80**:117–132.
12. Hearn G, Testa RB. Modal analysis for damage detection in structures. *Journal of Structural Engineering* 1993; **117**:1798–1803.
13. Shi ZY, Law SS, Zhang LM. Structural damage localization from modal strain energy changes. *Journal of Sound and Vibration* 1998; **218**:825–844.
14. Cornwell P, Doebling SW, Farrar CR. Application of the strain energy damage detection method to plate-like structures. *Journal of Sound and Vibration* 1999; **224**:359–374.
15. Simon M, Tomlison GR. Use of the Hilbert transform in the modal analysis of linear and non-linear structure. *Journal of Sound and Vibration* 1984; **96**:421–436.
16. Tomlinson GR, Ahmed I. Hilbert transform procedures for detecting and quantifying non-linearities in modal testing. *Meccanica* 1987; **22**:123–132.
17. Feldman M. Non-linear free vibration identification via the Hilbert transform. *Journal of Sound and Vibration* 1997; **208**:475–489.

DOI: 10.1002/stc

18. Braun S, Feldman M. Time–frequency characteristics of non-linear systems. *Mechanical Systems and Signal Processing* 1997; **11**:611–620.
19. Prime MB, Shevitz DW. Linear and nonlinear method for detecting cracks in beams. *Proceedings of the 14th International Modal Analysis Conference*, Dearborn, MI, February 1996; 1437–1443.
20. Feldman M, Seibold S. Damage diagnosis of rotors: application of Hilbert transform and multihypothesis testing. *Journal of Vibration and Control* 1999; **5**:421–442.
21. Yang JN, Lin S, Pan S. Damage identification of structures using Hilbert–Huang spectral analysis. *Proceedings of the 15th ASCE Engineering Mechanics Conference*, Columbia University, New York, NY, June 2002.
22. Huang NE, Shen Z, Long SR, Wu MLC, Shih EH, Zheng Q, Tung CC, Liu HH. The empirical mode decomposition and the Hilbert–Huang spectrum for nonlinear and non-stationary time series analysis. *Proceedings of the Royal Society* 1998; **A 454**:903–995.
23. Huang NE, Wu MLC, Long SR, Shen Z, Qu W, Gloersen P, Fan KL. A confidence limit for the empirical mode decomposition and Hilbert spectral analysis. *Proceedings of the Royal Society* 2003; **A 459**:2317–2345.
24. Yang JN, Lei Y, Pan S, Huang NE. System identification of linear structure based on Hilbert–Huang spectral analysis. Part 1: normal modes. *Earthquake Engineering and Structural Dynamics* 2003; **32**:1443–1467.
25. Nocedal J, Wright SJ. *Numerical Optimization*. Springer: New York; 1999.
26. Dennis JE, Schnabel RB. *Numerical Methods for Unconstrained Optimization*. SIAM: Philadelphia, PA; 1996 (Original volume 1983).
27. Oppenheim AV, Schafer RW. *Discrete-Time Signal Processing*. Prentice-Hall: Englewood Cliffs, NJ; 1989.
28. Lo Iacono F, Navarra G, Pirrotta A. Experimental validation of a damage identification procedure based on the analytical signal. *Proceedings of the International Symposium on Recent Advances in Mechanics, Dynamical Systems and Probability Theory, MDP—2007*, Palermo, June 3–6, 2007.

DOI: 10.1002/stc